Published in final edited form as:
Cancer Res. 2009 February 15; 69(4): 1459–1468. doi:10.1158/0008-5472.CAN-08-2628.

TUMOR AND VASCULAR TARGETING OF A NOVEL ONCOLYTIC MEASLES VIRUS RETARGETED AGAINST THE UROKINASE RECEPTOR

Yuqi Jing[1], **Caili Tong**[2], **Jin Zhang**[1,*], **Takafumi Nakamura**[2,+], **Ianko Iankov**[2], **Stephen J. Russell**[2], and **Jaime R. Merchan**[1]

[1]Division of Hematology-Oncology, University of Miami Miller School of Medicine and Sylvester Comprehensive Cancer Center, Miami FL 33136

[2]Department of Molecular Medicine, Mayo Clinic Rochester, MN 55905.

Abstract

Oncolytic measles virus (MV) induces cell fusion and cytotoxicity in a CD46 dependent manner. Development of fully retargeted oncolytic MVs would improve tumor selectivity. The urokinase receptor (uPAR) is a tumor and stromal target overexpressed in multiple malignancies. MV-H glycoproteins fully retargeted to either human or murine uPAR were engineered and their fusogenic activity was determined. Recombinant human (MV-h-uPA) and murine (MV-m-uPA) uPAR retargeted MVs expressing eGFP were rescued and characterized. Viral expression of chimeric MV-H was demonstrated by RT-PCR and Western Blot. In vitro viral replication was comparable to MV-GFP control. Receptor and species specificity of MV-uPAs were demonstrated in human and murine cells with different levels of uPAR expression. Removal of the ATF ligand from MV-uPA -by Factor Xa treatment- ablated MV-uPA's functional activity. Cytotoxicity was demonstrated in uPAR expressing human and murine cells. MV-h-uPA efficiently infected human endothelial cells and capillary tubes in vitro. Intravenous administration of MV-h-uPA delayed tumor growth and prolonged survival in the MDA-MB-231 breast cancer xenograft model. Viral tumor targeting was confirmed by immunohistochemistry. MV-m-uPA transduced murine mammary tumors (4T1) in vivo, after intratumor administration. MV-m-uPA targeted murine tumor vasculature after systemic administration, as demonstrated by dual (CD31 and MV-N) staining of tumor capillaries in the MDA-MB-231 model. In conclusion, MV-uPA is a novel oncolytic MV associated with potent and specific antitumor effects and tumor vascular targeting. This is the first retargeted oncolytic MV able to replicate in murine cells and target tumor vasculature in an uPAR dependent manner.

Introduction

Oncolytic virotherapy is an innovative biological strategy that holds great promise for the treatment of cancer. Because oncolytic viruses could in principle be genetically engineered to specifically target, replicate in, and ultimately kill tumor cells, they may offer advantages over conventional treatments (1,2). The Edmonston vaccine strain of measles virus (MV-Edm) (3) is a novel oncolytic virus currently being evaluated in phase I clinical trials in ovarian cancer, multiple myeloma and glioblastoma multiforme (http://www.clinicaltrials.gov). MV-Edm exerts its cytopathic effects by formation of multinuclear cell aggregates, i.e., syncytia,

Corresponding author: Jaime R. Merchan. Division of Hematology-Oncology, University of Miami Miller School of Medicine. 1475 NW 12th Avenue, Suite 3300. Miami, FL 33136. E-mail: jmerchan2@med.miami.edu.
+Present address: Department of Molecular Genetics, Medical Institute of Bioregulation, Kyushu University, Fukuoka 812-8582, Japan.
*Present address: Invitrogen Corporation. 7335 Executive Way Frederick, MD 21704

resulting from fusion of infected cells (1). Cell fusion is mediated by the MV-H glycoprotein, which binds to the endogenous MV-Edm cell surface receptor CD46, and signals to MV-F to trigger cell fusion. As fusion progresses, surrounding nontransfected cells are recruited into expanding syncytia, generating a significant local bystander effect (4,5).

Even though measles virus-induced cytopathic effects seem to preferentially affect tumor cells, normal cells could also be affected (6–8), limiting the therapeutic potential of these agents. A desirable target for an oncolytic virus should be biologically relevant, overexpressed by tumors and tumor stromal cells, to potentially amplify the virus'antitumor effects. Development of oncolytic viruses against murine tumor targets would allow the testing of retargeted oncolytic viruses in syngeneic cancer models in order to characterize and predict virus-tumor-host interactions that may be relevant for human clinical studies.

The plasminogen activator (PA) system consists of a family of proteases (urokinase-uPA-tissue plasminogen activator-tPA-, plasmin), receptors and inhibitors, and is involved in the regulation of coagulation, angiogenesis, and tumor growth (9–12). The importance of the PA system in breast and other human malignancies is well established (13–15). Binding of uPA with its receptor (uPAR) initiates a proteolytic cascade that results in the conversion of plasminogen to plasmin, extracellular matrix degradation and activation of matrix metalloproteinases (10). Functionally, uPA can be divided into three independent regions: an amino-terminal epidermal growth factor (EGF)-like domain, a kringle domain and a carboxy-terminal catalytic domain (16). The first two domains comprise the amino-terminal fragment (ATF). The receptor-binding module resides in the EGF-like domain, in residues 21–32 (17).

The urokinase receptor (uPAR) is a three-domain (D1, D2 and D3) glycosyl phosphatidylinositol (GPI)-anchored protein with a high affinity (1 nM) for uPA, pro-uPA and the ATF (18). The molecular role of uPAR in cancer progression is well characterized. In addition to its participation in extracellular matrix degradation, uPAR elicits a number of -non-proteolytic- cellular responses involved in tumor progression and angiogenesis, such as cell migration, adhesion, differentiation and proliferation (19–22). uPAR is overexpressed in breast tumor cells as well as in tumor stroma, and its presence has been associated with an aggressive tumor phenotype and adverse prognosis (21,23–26). Moreover, preclinical studies have demonstrated that targeting the uPAR, by monoclonal antibodies or antisense oligonucleotides, is a promising -tumor selective- strategy for the treatment of uPAR overexpressing tumors (27–29).

In the present study, we report on the generation and characterization of fully retargeted oncolytic measles viruses against the human and murine urokinase receptor, as well as the assessment of their tumor and endothelial targeting abilities in vitro and in vivo.

Materials and Methods

Cell culture

Vero (african green monkey kidney), NIH-3T3 (immortalized mouse fibroblasts), CHO (chinese hamster ovary), 786-O (human renal carcinoma), MC38 (murine colon carcinoma), CT-26 (murine colon cancer), Hep3B (human hepatoma cell lines) and MDA-MB-468 (human breast carcinoma) cells were purchased from the American Type Culture Collection (ATCC, Manassas, VA) and maintained in Dulbecco's modified Eagle's medium (DMEM) containing 10% fetal bovine serum (FBS). HT1080 (human fibrosarcoma cells) and MDA-MB-231 (human breast cancer) cells were obtained from ATCC, and maintained in RPMI-1640 with 10% FBS. 4T1 (murine mammary carcinoma) cells, gifts of Dr. Carlos Arteaga (Vanderbilt University, Nashville, TN), NIH 3T3/RAS cells, gifts of Dr. Y. Ikeda (Mayo Clinic, Rochester, MN) and Vero-αHis cells (30) were maintained in DMEM with 10% FBS. The rescue helper

cell line 293-3–46 (30) was grown in DMEM with 10% FBS and 1.2 mg/ml of G418 (Invitrogen, Carlsbad, CA). CASMC (coronary artery smooth muscle cells), HMEC (human mammary epithelial cells), HUVEC (human umbilical vein endothelial cells) and HDF (human dermal fibroblasts) were purchased from Lonza (Walkersville, MD) and maintained in growth medium as recommended by the vendor. All cells were grown at 37°C and 5% CO_2.

Generation of stable uPAR overexpressing and knockdown cell lines

Total RNA was isolated from 4T1 cells using the RNeasy Mini Kit (Qiagen, Valencia, CA). The cDNA encoding murine uPAR was obtained by RT-PCR as a *BamHI/Not*I fragment using the following primers: (forward) 5'-TTTGGATCCATCATGGGACTCCCAAGG, (reverse) 5'-TTTGCGGCCGCTCAG GTCCAGAGGAGGACG-3'. The purified PCR product was cloned into the *BamH*I-*Not*I site of the lentiviral vector pHR-SIN-CSGWd1NotI, a gift of Dr. Ikeda, and the cDNA sequence was verified. Lentiviral packaging was performed as previously reported (30). CHO cells were infected with lentivirus and clones expressing high levels of murine uPAR were sorted by FACS. Stable uPAR knockdown 4T1 cells were generated using vectors containing microRNA based shRNA targeting mouse uPAR, and non-silencing control vectors (OpenBiosystems, Huntsville, AL). Vectors were delivered into 4T1 cells using arrest-in transfection reagent (Open Biosystems) following the manufacturer's recommendations. The levels of expression of uPAR were analyzed using real time PCR (Applied Biosystems, Foster City, CA) and flow cytometry.

Flow cytometry

Cells were harvested by cell dissociation buffer (Invitrogen) and the surface expression of relevant receptors was detected using anti-mouse or human uPAR FITC-conjugated antibody (R&D systems, Minneapolis, MN) and anti-human CD46 FITC-conjugated antibody (Abcam, Cambridge, MA). Washed cells were analyzed on a Becton-Dickinson FACScan Plus cytometer and analyzed using CellQuest software (Becton-Dickinson, San Jose, CA). Data were displayed as flow cytometric histograms of approximately 5000 events. Relative changes in cell surface uPAR or CD46 expression levels were determined by quantitative assessment of fluorescence shifts (from flow cytometry data), using WinMDI 2.9 software (J. Trotter, Scripps Research Institute, La Jolla, CA) and expressed as fold changes of the mean fluorescence index (MFI).

Construction of chimeric measles virus (MV) H glycoproteins retargeted against the urokinase receptor

Total RNA was isolated from 786-O cells. The cDNA encoding human uPA was obtained by RT-PCR using the following primers: (forward) 5'-TTTGCTAGCATCATGAGAGCCCTGCTGGCG, (reverse) 5'-TTTTGCGGCCGCTCA GAGGGCCAGGCCATT-3'. The cDNA was cloned into the *Nhe*I-*Not*I site of pcDNA3.1(+) (Invitrogen). The amino terminal fragment (ATF) of human uPA was amplified as a *Sfi*I/*Not*I fragment by PCR from pcDNA3.1(+)-huPA using the following primers: (forward) 5'-GGCCCAGCCGGCCAGCAATGAACTTCATCA-3', (reverse) 5'-TGCGGCCGCTTTTCCATCTGCGCAGTCATG-3'. ATF of mouse uPA was amplified by PCR from pcDNA3.1(+)-muPA (31) using the following primers: (forward) 5'-GGCCCAGCCGGCCGGCAGTGTACTTGGA-3', (reverse) 5'-TGCGGCCGCGCTA AGAGAGCAGTCATGCACCATGCA-3'. Human and murine uPA-ATFs were cloned into the *Sfi*I and *Not*I cloning sites of $pTNH6_{AALS}$ respectively, and verified by DNA sequencing. The constructs containing the chimeric MV-H glycoproteins were named $pTNH6_{AALS}$-h-ATF (targeting human uPAR) and $pTNH6_{AALS}$-m-ATF (targeting murine uPAR), respectively.

Cotransfections and cell fusion assay

Cells (2×10^5/well) were seeded in each well of 6-well plates. After overnight incubation, cells were cotransfected with 0.5 μg pCGF, a measles F expression plasmid and 0.5 μg of the chimeric pTNH6$_{AALS}$-ATF constructs using Effectene transfection reagent (Qiagen). At 48 h after transfection, the syncytia were photographed using inverted microscope (Nikon, Melville, NY).

Construction of MV-uPA, virus rescue, propagation, titration and infection

Retargeted MV-H glycoproteins from pTNH6$_{AALS}$-h-ATF and pTNH6$_{AALS}$-m-ATF were inserted into the *Pac*I and *Spe*I sites of p(+)MV-eGFP, which encodes the full-length infectious clone of MV-Edm, resulting in p(+)MV-h-uPA and p(+)MV-m-uPA construct (Fig 1*A*). The rescue of MV-uPA virus employing the pseudoreceptor STAR system, the preparation of virus stocks, in vitro virus propagation, titration, and infection were performed as previously reported (32).

Reverse transcription-PCR

Vero-αHis cells (2×10^5) were infected with recombinant MVs (MOI: 0.5) in a 6-well plate. After 48h incubation, total RNA was extracted. RT-PCR was done using Qiagen one-step RT-PCR kit. The primers used to detect chimeric MV-H gene were 5-AGGGTGCAAGATCATCCA-3 (Forward), 5-CTGTAAGCGTGAGGGAG-3 (Reverse).

Immunoblot analysis of viral H protein

Viral samples (10^5 TCID50) were mixed with an equal volume of SDS loading buffer. Samples were fractionated on a 7.5% SDS-polyacrylamide gel (Bio-Rad, Hercules, CA) and immunoblotted with anti-measles H protein antibody at 1:10000 dilution (a generous gift from R. Cattaneo, Mayo Clinic). A goat anti-rabbit-HRP second antibody (Millipore, Temecula, CA) was applied, and the peroxidase activity was revealed with the enhanced chemiluminescence system (Amersham Bioscience, Piscataway, NJ).

Matrigel tube formation assay and infection with viral particles

The matrigel tube formation assay was performed as previously described (33,34). When HUVEC tubes were formed (16 hours after HUVEC plating into matrigel coated wells), they were infected with either MV-Edm or MV-h-uPA diluted in Opti-MEM at a MOI = 1 for 2 hours. After 2 hours, medium containing the virus was removed and endothelial growth medium (EGM-2) was added. Infection efficiency was measured as mean fluorescence intensity in arbitrary units by NIS-Elements image analysis software (Nikon). Experiments were done in triplicate.

Assessment of in vitro cytopathic effects

Cells were plated in six-well plates at a density of 10^5 per well. 24 hours after seeding, the cells were infected at MOI = 1 in 1 mL of Opti-MEM for 2 hours at 37°C. The same number of uninfected cells in six-well plates was used as controls. At 48h, 72h and 96h after infection, the number of viable cells (determined by tryptan blue exclusion) in each well was counted using Vi-Cell cell viability analyzer (Beckman Coulter, Fullerton, CA). The percentage of surviving cells was calculated by dividing the number of viable cells in the infected well by the number of viable cells in the uninfected well corresponding to the same time point, as previously reported (35,36). Infection was confirmed using fluorescent microscopy (Nikon) at the corresponding time points.

In vivo experiments to test the oncolytic activity of retargeted measles viruses

Animal studies were approved by Institutional Animal Care and Use Committee of University of Miami and the Mayo Clinic. Human breast cancer xenografts were established by inoculating MD-MBA-231 cells (2×10^6 cells in 50 μl PBS) using 27 gauge needle into the fifth mammary fat pad of 9–10-week-old female immunodeficient (NOD/SCID) mice (Jackson Labs, Bar Harbor, ME). When tumors reached a diameter of 0.4–0.5 cm, animals were randomized into 2 groups (n = 10 per group) and received seven intravenous injections of either MV-h-uPA at 1×10^6 TCID50 in 50 μl Opti-MEM (treatment group) or equal volumes of Opti-MEM alone (mock therapy group), on days 0, 2, 4, 7, 9, 12 and 14. Tumor bearing animals were followed until they reached sacrifice criteria (when tumor burden reached 10% of body weight, if tumor ulceration occurred or mice became moribund). Tumor size was measured every third day and the volume (product of $0.52\times\text{length}\times\text{width}^2$) was recorded.

In vivo experiments for detection of measles

For assessment of tumor targeting after intravenous viral administration, human breast cancer xenografts were established as above. When the tumors reached 0.6 cm in diameter, mice received two intravenous injections (three days apart) of recombinant MVs at 1.5×10^6 TCID50 in 50 μl Opti-MEM. 72 hours after the last treatment, tumors were resected and frozen for further studies. For assessment of in vivo viral transduction in a murine mammary cancer model, 2×10^5 of 4T1 cells in PBS were implanted subcutaneously into the fifth mammary fat pad of 9–10-week-old female SCID (n=3) and immunocompetent (n = 3) BALB/c mice (Harlan Sprague-Dawley, Indianapolis, IN). When tumors have reached 0.5 cm in diameter, mice were given two intratumoral injections of MV-m-uPA at a dose of 1×10^6 TCID50. 48 hours after the last treatment, mice were sacrificed and tumors were resected. eGFP expression of fresh tumor sections was analyzed by a Zeiss LSM 410 laser scanning confocal microscope (Carl Zeiss, Thornwood, NY).

Immunohistochemistry studies

Frozen tumor sections were used for immunostaining for measles N protein and CD31. Reagents were obtained from Vector Laboratories (Burlingame, CA) when otherwise specified. Cryostat sections were fixed in cold acetone for 10 min and endogenous peroxidase activity was quenched with 0.3% H_2O_2 for 10 min. The slides were incubated with biotinylated mouse anti-MV-nucleoprotein antibody (Chemicon International, Temecula, CA) for 30 min at 37°C. The slides were developed with VECTASTAIN ABC–alkaline phosphatase (AP) kit and an AP substrate kit. For dual staining (MV-N and CD31) of tumor capillaries, slides were prepared as above and incubated with biotinylated antibodies to murine CD31 (BD Biosciences Pharmingen, San Diego, CA). Positive staining was visualized with a VECTASTAIN ABC (HRP) kit and 3, 3, 9-diaminobenzidine (DAB) substrate. The slides were then treated with an avidin blocking kit, washed in PBS and incubated with biotinylated mouse anti-MV-nucleoprotein antibody for 30 min at 37°C. After washing in PBS, the slides were developed with VECTASTAIN ABC–AP kit and an AP substrate kit.

Statistical analysis

In vitro data are presented as means +/− standard deviations. Results from in vivo studies are shown as means +/− standard error of the mean. Statistical analysis among groups was performed by analysis of variance followed by Tukey-Kramer, Fisher's or Wilcoxon rank sum test, and $p < 0.05$ was considered to be statistically significant. Overall survival was analyzed by the Kaplan–Meier method and differences were analyzed by the log-rank test. All statistical tests were two-sided.

RESULTS

Functional activity of chimeric MV-H glycoproteins retargeted against uPAR

Human and murine uPAR retargeted MV-H glycoproteins were generated by displaying ATF of human and murine uPA, respectively, at the C-terminus of $pTNH_{AALS}$ (Fig.1*A*). Functional activity of the chimeric MV-H glycoproteins was assessed by co-transfection assays. Human and murine $pTNH_{AALS}$-ATF induced cell fusion and syncytia formation in human (MDA-MB-468, HT-1080) and murine (3T3) tumorigenic cells, respectively (Fig. 1*B*, supplementary table S. 1 and figure S. 1). Non-cancer cells (CASMCs) and cancer cells not overexpressing uPAR did not undergo cell fusion (Fig. 1*B*, table S.1 and Fig. S. 1).

Rescue and in vitro characterization of recombinant oncolytic MVs fully retargeted against human and murine uPAR

Once feasibility of uPAR dependent cell fusion was demonstrated, oncolytic MVs fully retargeted against human and murine uPAR were engineered (Fig. 1*A*) and rescued. Human and murine versions of MV-uPA were generated because of species specificity differences between human and murine uPAR and ATF, where human urokinase (ATF) doesn't bind to murine uPAR and vice versa (37). Expression of the chimeric MV-H glycoproteins (of larger size than unmodified MV-H) was demonstrated at the RNA level, by RT-PCR of Vero-αHis cells exposed to the recombinant viruses (Fig. 1*C*.I), and at the protein level, by western blot of MV-H in naked viral particles (Fig. 1*C*.II). In vitro viral propagation was assessed by the previously described one step growth curve (38). The retargeted viruses propagated efficiently in Vero-αHis cells, in a His dependent manner, compared to (unmodified) MV-GFP control virus.

Receptor and species specificity of MV-uPA

To assess uPAR species specificity, human and murine cancer cells overexpressing uPAR were infected with human or murine retargeted oncolytic measles viruses. MDA-MB-231 cells were sensitive to MV-GFP and MV-h-uPA induced cell fusion, but resistant to MV-m-uPA (Fig. 2*A*). MC-38 cells were resistant to unmodified MV-GFP and MV-h-uPA (Fig. 2*B*). MV-m-uPA, however, efficiently infected MC-38 cells and induced cell fusion (Fig. 2*B*).

MV-uPA's receptor specificity was assessed by the following experiments: First, the ATF ligand was removed from the retargeted virus by factor X(a) treatment of MV-h-uPA. Western blot analysis showed successful cleavage of the linker and separation of the ATF fragment of uPA from MV-H glycoprotein (Fig. 2*C*, western blot, second vs. fourth lane). Factor X(a) treated MV-h-uPA, but not mock treated virus, lost its ability to induce cell fusion in MDA-MB-231 cells (compare Fig. 2*C*. 4 vs. 2*C*. 2), confirming that MV-h-uPA induced cell fusion is dependent on binding of MV-H-ATF to uPAR. Factor X(a) treatment of MV-GFP did not affect cell fusion (compare Fig. 2*C*. 1 with Fig. 2*C*. 3).

Next, CHO cells and CHO-muPAR cells were exposed to MV-m-uPA (Fig. 2*D*). MV-m-uPA infection of CHO cells, which do not express mouse uPAR (they express hamster uPAR) resulted in modest cell fusion (Fig 2*D*. 1); CHO-muPAR cells, on the other hand, underwent cell fusion and syncytia formation upon infection with MV-m-uPA (Fig. 2*D*. 2). MV-GFP and MV-h-uPA did not induce significant cell fusion in CHO cells (data not shown).

Finally, 4T1 cells were exposed to MV-m-uPA and syncytia were observed (Fig. 2*D*. 3). 4T1-muPAR knockdown cells became less susceptible to infection with MV-m-uPA (Fig. 2*D*. 4). The above data clearly demonstrate that human and murine MV-uPA enter cells and induce cell fusion/syncytia formation in an uPAR dependent and species specific manner.

uPAR dependent in vitro endothelial cell and capillary infection

The importance of uPAR during angiogenesis is well established, with its role in migration, invasion and cell signaling (16,39–41). uPAR expression was upregulated in HUVEC cells stimulated with 2% serum and angiogenic growth factors, as compared to HUVECs maintained in basal conditions (Fig. 3*B*). Levels of CD46 (MV-Edm's natural receptor) did not significantly change after HUVEC exposure with EGM-2 (Fig. 3*A*). Increased uPAR expression after stimulation of HUVEC monolayers was associated with more efficient infection by MV-h-uPA (mean fluorescent intensity= 312,826 +/− 25,379; Fig. 3*C*. 2) compared to the unmodified MV-GFP control (mean fluorescent intensity= 102,558 +/−21,567, $p < 0.001$; Fig. 3*C*. 1). Next, the ability of MV-h-uPA to infect capillary tubes was assessed. HUVEC capillary tubes were exposed to MV-h-uPA. Compared to MV-GFP, MV-h-uPA was associated with more efficient capillary infection, as evidenced by more frequent fluorescent capillary tubes (higher mean fluorescence intensity= 53,040 +/−8,356) induced by the retargeted versus the control virus (mean fluorescence intensity= 11,497 +/− 2,393, $p < 0.001$; Fig. 3*C*. 4 and 6 vs. Fig. 3*C*. 3 and 5).

In vitro cytopathic effects

Human and murine cancer cell lines were exposed to the recombinant viruses, and cell viability was determined at different timepoints by tryptan blue exclusion (35,36). In human cancer cells (MDA-MB-231 and 786-O), MV-h-uPA and MV-GFP induced significant ($p < 0.001$, Tukey-Kramer test) cytotoxicity at 48, 72, and 96 hours, compared to MV-m-uPA (Fig. 4*A*, *B*). The cytopathic effects of MV-h-uPA were more prominent than MV-GFP (72 hour cytotoxicity: 84% vs 74% in MDA-MB-231 cells and 79% vs. 70% in 786-O cells, respectively). MV-m-uPA, on the other hand, induced significant cytotoxicity ($p < 0.001$, Tukey-Kramer test) in the murine tumorigenic cell lines 4T1 (72 hour cytotocixity= 64%; Fig. 4*C*) and 3T3 Ras (72 hour cytotoxicity= 57%; Fig. 4*D*), compared to MV-h-uPA (cytotoxicity= 7% and 16% in 4T1 and 3T3 Ras, respectively). Murine cell lines were resistant to MV-GFP, as they do not express human CD46 (cytotoxicity: 2% and 5% in 4T1 and 3T3 Ras, respectively).

In vivo antitumor effects and in vivo tumor targeting

To determine whether the in vitro cytopathic effects are relevant on human breast cancer in vivo, recombinant oncolytic viruses were administered systemically into (MDA-MB-231) tumor bearing mice. MV-h-uPA treatment was associated with significant antitumor effects compared to mock treatment (Fig. 5*A*) Tumor growth in MV-h-uPA treated mice was inhibited by 76% at day 39 ($p= 0.0009$, Wilcoxon ranks sum test). Significant prolongation of survival was observed in mice treated with MV-h-uPA compared to mock (80 day survival rate in the control group= 0%, versus 70% in the MV-h-uPA treated group; median survival in control group= 63 days -95% CI= 42–70 days- vs. median survival not reached in the MV-h-uPA treated group by the end of the study −100 days-; $p= 0.0039$, log rank test; Fig. 5*B*). Systemic administration of MV-h-uPA was not associated with acute or subacute toxicity in tumor bearing mice during or after intravenous administration.

Tumor targeting of the recombinant viruses after systemic administration of the viral agent was assessed in additional groups of tumor bearing mice. They were treated with two intravenous injections of recombinant measles viruses, and tumors were resected for immunohistochemistry studies for MV-N protein. As shown in Fig. 5*C*, viral protein was detected in the tumors treated with intravenous MV-h-uPA, but not in the mock treated tumors, confirming the in vivo tumor targeting abilities of MV-h-uPA after systemic administration.

In vivo murine tumor transduction and tumor vascular targeting of MV-m-uPA

In vitro viral replication of MV-m-uPA was demonstrated in Fig. 1*D*, in Vero-αHis (monkey) cells, in a His-dependent manner. To demonstrate replication of MV-m-uPA in a murine uPAR dependent manner, the one step replication curve was performed in NIH 3T3 cells infected with MV-m-uPA. As seen in Fig. 6*A* and *B*, MV-m-uPA was able to replicate in the murine tumorigenic cells, demonstrating murine uPAR dependent viral replication in vitro. Replication of MV-m-uPA in murine cells however, was less efficient than its replication in Vero-αHis cells.

To evaluate in vivo viral transduction in a syngeneic model, BALB/C mice bearing 4T1 tumors were injected with MV-m-uPA intratumorally. Fresh tumors were sectioned and examined by laser confocal microscopy. Tumors treated with MV-m-uPA showed GFP positive structures, consistent with intratumor syncytia (Fig. 6*C*. 1, 2 and supplementary fig. S.2*C* -SCID mice- and Fig. 6*C*. 3 and supplementary fig. S.2. B-immunocompetent mice). Tubular GFP positive structures were identified, resembling infected tumor capillary structures (Fig. 6*C*. 3). This data strongly suggests successful in vivo viral transduction in a murine uPAR dependent manner. No signs of acute toxicity were observed in mice after intratumoral treatment with MV-m-uPA.

To assess the ability of MV-m-uPA to target tumor vasculature in vivo, mice bearing MDA-MB-231 tumors were injected systemically with MV-m-uPA, and double staining for MV-N protein and CD31 in tumor capillaries was performed on resected tumors. As shown in Fig. 6*D*. 3 (and supplementary fig. S.3*C, F, I*), after systemic administration of MV-m-uPA in tumor bearing mice, strong staining for MV-N protein (blue) was observed around tumor capillaries (CD31= brown). Tumor capillaries from mice treated with vehicle control, or MV-GFP stained positive for CD31, but did not stain for MV-N (Fig. 6*D*. 1, and Fig. S.3*A, D, G* for vehicle control; Fig. 6*D*. 2, and Fig. S.3*B, E, H* for MV-GFP). Because MV-m-uPA does not efficiently bind to MDA-MB-231 cells (which express human uPAR, Fig. 2*A*), the above findings demonstrate the ability of the murine version of MV-uPA to target murine tumor capillaries in vivo, in an uPAR dependent manner, after systemic administration. Importantly, we did not observe any acute toxicity in tumor bearing mice treated with two intravenous injections of the murine uPAR retargeted oncolytic virus (MV-m-uPA), suggesting safety and specificity of the murine retargeted oncolytic virus after systemic administration.

DISCUSSION

In this report, we successfully rescued and characterized a novel Edmonston vaccine strain oncolytic measles virus (MV-Edm) fully retargeted against the urokinase receptor (uPAR), a highly relevant tumor and tumor stromal target (42,43). uPAR retargeted MVs were generated by displaying the uPAR binding amino terminal fragments (ATF) of either human (MV-h-uPA) or murine (MV-m-uPA) uPA into the C-terminus of a mutant MV-H glycoprotein (H_{AALS}) (32) that lacks the ability to attach to its endogenous receptors. We demonstrated that the human and murine uPAR retargeted viral agents were able to attach to, replicate, and induce cell fusion and cytotoxicity in a receptor and species specific manner. MV-h-uPA significantly delayed tumor progression and improved survival in a breast cancer xenograft model. Finally, we presented evidence that MV-h-uPA can efficiently infect activated endothelial cells and that MV-m-uPA can transduce murine tumors and target tumor capillaries in vivo.

Clinical development of fully retargeted oncolytic MVs requires a comprehensive assessment of the pharmacokinetic and pharmacodynamic properties of the viral agents in appropriate preclinical models. This information will be important to predict potential safety or biodistribution issues before human testing. Previously reported oncolytic MVs redirected against tumor targets such as CD38, EGFR, EGFR-VIII have shown potent antitumor effects

(7,32,44). However, full development of these agents into phase I trials is hindered by the inability to test these viruses in syngeneic cancer models, as the above agents cannot replicate in murine cells. Attempts have been made to generate targeted oncolytic MVs to be used in syngeneic cancer models. Ungerechts et al. reported on the activity of MV-PNP-antiCEA against murine colon tumors expressing human CEA(45). However, because murine tissues do not express human CEA, studies to predict virus-host-tumor interactions and tissue biodistribution are not possible, and the in vivo utility of MV-PNP-antiCEA is limited to murine tumors artificially expressing CEA. MV-uPA is the first oncolytic measles virus retargeted against a tumor target (uPAR) that is relevant for, and naturally expressed in human and murine tumors. Because MV-m-uPA can infect and transduce murine tumors in vitro and in vivo, it provides a valuable tool to address important issues relevant to the safety and biodistribution of the viral agents in unmodified, immunocompetent murine models of cancer naturally expressing uPAR, in a way that may more closely resemble the human cancer situation.

The tumor endothelium represents a barrier to the effective delivery of therapeutic agents into tumor cells (46). Because endothelial cells are easily accessible after intravenous administration of a therapeutic agent, oncolytic viruses that target tumor endothelium may have the advantage of circumventing this problem, since they may bind to endothelial cells, replicate in them, and facilitate viral entry into tumor tissue (46,47). In this report, we showed that human endothelial uPAR expression is increased upon stimulation with serum and endothelial growth factors (Fig. 3*B*). This is concordant with previous reports suggesting that VEGF or tumor cell conditioned medium up regulate endothelial uPAR expression (40,48), and emphasize the importance of uPAR in tumor angiogenesis (41,48). Under those conditions, MV-h-uPA infects HUVEC monolayers and capillary tubes (in matrigel) more efficiently than the unmodified MV-Edm. Importantly, systemic administration of MV-m-uPA successfully targeted and infected tumor vasculature, as evidenced by positive double staining (CD31 and MV-N) of tumor capillaries in MV-m-uPA treated mice (Fig. 6*D*. 3 and Fig. S.3*C, F, I*)), as compared to controls (Fig. 6*D*. 1, 2 and Fig. S.3*A, D, G* and *B, E, H*). This provides first time evidence of the ability of a murine retargeted oncolytic virus to reach the tumor vascular compartment in vivo, after intravenous administration.

A previous study reported on the activity of an oncolytic MV-Edm (called “MV-ERV”) displaying echistatin, a disintegrin that binds to αvβ3 (38). Antitumor effects and in vivo capillary infection were shown by *local* administration of MV-ERV into tumors or chick chorioallantoic membranes, respectively. MV-uPA differs from MV-ERV in that it induced antitumor effects (MV-h-uPA) and tumor vascular targeting (MV-m-uPA) in vivo after *systemic* administration (Fig. 6*D*. 3). Moreover, intravenous administration of MV-m-uPA in tumor bearing mice was safe, whereas safety of MV-ERV after systemic administration was not assessed.

Even though we have achieved the important goal of rescuing and characterizing a murine retargeted oncolytic MV, which is safe and able to target tumor vasculature in vivo, a number of questions are raised in this study. MV-m-uPA replicates in murine cells in vitro (Fig. 6*A, B*), however, the efficiency of viral replication (viral titers) in rodent cells is lower than its replication in non-murine (e.g. Vero-α His) cells (Fig. 1*D*). This suggests the presence of intracellular restriction mechanisms to replication and generation of progeny virus in rodent cells that need to be addressed in future studies. Second, uPAR is expressed in a number of normal tissues, potentially raising issues regarding specificity and safety of targeting this receptor. Tumor selectivity of uPAR directed therapies has been demonstrated by Rabbani et al., who showed in rat models of cancer that anti-rat uPAR antibodies specifically target tumor tissues and are able to detect occult tumor metastases in vivo (29). Such tumor selectivity may be explained by the fact that uPAR expression is significantly higher in tumor and tumor stroma, compared to normal tissues (42, 43, 49). Induction of uPAR expression by activated

endothelium provides an additional advantage for MV-uPA, by increasing its ability to bind to tumor capillaries. Finally, we found that intratumor or intravenous administration of MV-m-uPA was not associated with acute toxic effects in tumor bearing mice.

In summary, this study demonstrates successful rescue and characterization of an uPAR retargeted measles virus, evidence of successful infection and replication in a receptor and species specific manner, and for the first time, the ability of a murine retargeted virus to reach murine tumor vasculature safely and efficiently. MV-uPA is a highly promising retargeted oncolytic virus with the potential of becoming an important novel therapeutic agent against breast cancer and other uPAR overexpressing malignancies. Studies aimed at overcoming barriers to viral replication in vitro and in vivo, and characterizing the virus-host-tumor interactions in syngeneic, immunocompetent models of cancer are underway.

Supplementary Material

Refer to Web version on PubMed Central for supplementary material.

Acknowledgements

This work was supported by the Susan G. Komen Foundation (J.R.M.), the Braman Family Breast Cancer Institute (J.R.M.), NIH R21 CA 119545-02(J.R.M.), the Sylvester Comprehensive Cancer Center (J.R.M.), Mayo Foundation (S.J.R.).

We would like to aknowledge Suzanne Greiner (Mayo Clinic) and Jaclyn Walbroehl (University of Miami) for their technical assistance.

REFERENCES

1. Fielding AK. Measles as a potential oncolytic virus. Rev Med Virol 2005;15:135–142. [PubMed: 15546127]
2. Nakamura T, Russell SJ. Oncolytic measles viruses for cancer therapy. Expert Opin Biol Ther 2004;4:1685–1692. [PubMed: 15461580]
3. Russell SJ. RNA viruses as virotherapy agents. Cancer Gene Ther 2002;9:961–966. [PubMed: 12522435]
4. Bateman A, Bullough F, Murphy S, et al. Fusogenic membrane glycoproteins as a novel class of genes for the local and immune-mediated control of tumor growth. Cancer Res 2000;60:1492–1497. [PubMed: 10749110]
5. Vile RG, Russell SJ, Lemoine NR. Cancer gene therapy: hard lessons and new courses. Gene Ther 2000;7:2–8. [PubMed: 10680008]
6. Hammond AL, Plemper RK, Zhang J, Schneider U, Russell SJ, Cattaneo R. Single-chain antibody displayed on a recombinant measles virus confers entry through the tumor-associated carcinoembryonic antigen. J Virol 2001;75:2087–2096. [PubMed: 11160713]
7. Peng KW, Donovan KA, Schneider U, Cattaneo R, Lust JA, Russell SJ. Oncolytic measles viruses displaying a single-chain antibody against CD38, a myeloma cell marker. Blood 2003;101:2557–2562. [PubMed: 12433686]
8. Nakamura T, Peng KW, Vongpunsawad S, et al. Antibody-targeted cell fusion. Nat Biotechnol 2004;22:331–336. [PubMed: 14990955]
9. Mazar AP, Henkin J, Goldfarb RH. The urokinase plasminogen activator system in cancer: implications for tumor angiogenesis and metastasis. Angiogenesis 1999;3:15–32. [PubMed: 14517441]
10. Choong PF, Nadesapillai AP. Urokinase plasminogen activator system: a multifunctional role in tumor progression and metastasis. Clin Orthop Relat Res 2003;415:S46–S58. [PubMed: 14600592]
11. Duffy MJ. The urokinase plasminogen activator system: role in malignancy. Curr Pharm Des 2004;10:39–49. [PubMed: 14754404]

12. Nakanishi K, Kawai T, Torikata C, Aurues T, Ikeda T. Urokinase-type plasminogen activator, its inhibitor, and its receptor in patients with upper urinary tract carcinoma. Cancer 1998;82:724–732. [PubMed: 9477106]
13. de Witte JH, Sweep CG, Klijn JG, et al. Prognostic value of tissue-type plasminogen activator (tPA) and its complex with the type-1 inhibitor (PAI-1) in breast cancer. Br J Cancer 1999;80:286–294. [PubMed: 10390010]
14. Chappuis PO, Dieterich B, Sciretta V, et al. Functional evaluation of plasmin formation in primary breast cancer. J Clin Oncol 2001;19:2731–2738. [PubMed: 11352966]
15. Fisher JL, Field CL, Zhou H, Harris TL, Henderson MA, Choong PF. Urokinase plasminogen activator system gene expression is increased in human breast carcinoma and its bone metastases--a comparison of normal breast tissue, non-invasive and invasive carcinoma and osseous metastases. Breast Cancer Res Treat 2000;61:1–12. [PubMed: 10930085]
16. Blasi F, Carmeliet P. uPAR: a versatile signalling orchestrator. Nat Rev Mol Cell Biol 2002;3:932–943. [PubMed: 12461559]
17. Appella E, Robinson EA, Ullrich SJ, et al. The receptor-binding sequence of urokinase. A biological function for the growth-factor module of proteases. J Biol Chem 1987;262:4437–4440. [PubMed: 3031025]
18. Ploug M, Ellis V. Structure-function relationships in the receptor for urokinase-type plasminogen activator. Comparison to other members of the Ly-6 family and snake venom alpha-neurotoxins. FEBS Lett 1994;349:163–168. [PubMed: 8050560]
19. Killeen S, Hennessey A, El Hassan Y, Waldron B. The urokinase plasminogen activator system in cancer: a putative therapeutic target? Drug News Perspect 2008;21:107–116. [PubMed: 18389102]
20. Cohen RL, Xi XP, Crowley CW, Lucas BK, Levinson AD, Shuman MA. Effects of urokinase receptor occupancy on plasmin generation and proteolysis of basement membrane by human tumor cells. Blood 1991;78:479–487. [PubMed: 1648983]
21. de Witte JH, Foekens JA, Brunner N, et al. Prognostic impact of urokinase-type plasminogen activator receptor (uPAR) in cytosols and pellet extracts derived from primary breast tumours. Br J Cancer 2001;85:85–92. [PubMed: 11437407]
22. Yebra M, Parry GC, Stromblad S, et al. Requirement of receptor-bound urokinase-type plasminogen activator for integrin alphavbeta5-directed cell migration. J Biol Chem 1996;271:29393–29399. [PubMed: 8910604]
23. Silvestri I, Longanesi I, Franco P, et al. Engaged urokinase receptors enhance tumor breast cell migration and invasion by upregulating alpha(v)beta5 vitronectin receptor cell surface expression. Int J Cancer 2002;102:562–571. [PubMed: 12447996]
24. Xing RH, Rabbani SA. Overexpression of urokinase receptor in breast cancer cells results in increased tumor invasion, growth and metastasis. Int J Cancer 1996;67:423–429. [PubMed: 8707419]
25. Qin W, Zhu W, Wagner-Mann C, Sauter ER. Nipple aspirate fluid expression of urokinase-type plasminogen activator, plasminogen activator inhibitor-1, and urokinase-type plasminogen activator receptor predicts breast cancer diagnosis and advanced disease. Ann Surg Oncol 2003;10:948–953. [PubMed: 14527916]
26. Grondahl-Hansen J, Peters HA, van Putten WL, et al. Prognostic significance of the receptor for urokinase plasminogen activator in breast cancer. Clin Cancer Res 1995;1:1079–1087. [PubMed: 9815897]
27. D'Alessio S, Margheri F, Pucci M, et al. Antisense oligodeoxynucleotides for urokinase-plasminogen activator receptor have anti-invasive and anti-proliferative effects in vitro and inhibit spontaneous metastases of human melanoma in mice. Int J Cancer 2004;110:125–133. [PubMed: 15054877]
28. Gondi CS, Lakka SS, Yanamandra N, et al. Adenovirus-mediated expression of antisense urokinase plasminogen activator receptor and antisense cathepsin B inhibits tumor growth, invasion, and angiogenesis in gliomas. Cancer Res 2004;64:4069–4077. [PubMed: 15205313]
29. Rabbani SA, Gladu J. Urokinase receptor antibody can reduce tumor volume and detect the presence of occult tumor metastases in vivo. Cancer Res 2002;62:2390–2397. [PubMed: 11956102]
30. Demaison C, Parsley K, Brouns G, et al. High-level transduction and gene expression in hematopoietic repopulating cells using a human immunodeficiency [correction of imunodeficiency] virus type 1-

based lentiviral vector containing an internal spleen focus forming virus promoter. Hum Gene Ther 2002;13:803–813. [PubMed: 11975847]

31. Merchan JR, Tang J, Hu G, et al. Protease activity of urokinase and tumor progression in a syngeneic mammary cancer model. J Natl Cancer Inst 2006;98:756–764. [PubMed: 16757700]
32. Nakamura T, Peng KW, Harvey M, et al. Rescue and propagation of fully retargeted oncolytic measles viruses. Nat Biotechnol 2005;23:209–214. [PubMed: 15685166]
33. Merchan JR, Chan B, Kale S, Schnipper LE, Sukhatme VP. In vitro and in vivo induction of antiangiogenic activity by plasminogen activators and captopril. J Natl Cancer Inst 2003;95:388–399. [PubMed: 12618504]
34. Merchan JR, Jayaram DR, Supko JG, He X, Bubley GJ, Sukhatme VP. Increased endothelial uptake of paclitaxel as a potential mechanism for its antiangiogenic effects: potentiation by Cox-2 inhibition. Int J Cancer 2005;113:490–498. [PubMed: 15455390]
35. Allen C, Vongpunsawad S, Nakamura T, et al. Retargeted oncolytic measles strains entering via the EGFRvIII receptor maintain significant antitumor activity against gliomas with increased tumor specificity. Cancer Res 2006;66:11840–11850. [PubMed: 17178881]
36. Phuong LK, Allen C, Peng KW, et al. Use of a vaccine strain of measles virus genetically engineered to produce carcinoembryonic antigen as a novel therapeutic agent against glioblastoma multiforme. Cancer Res 2003;63:2462–2469. [PubMed: 12750267]
37. Quax PH, Grimbergen JM, Lansink M, et al. Binding of human urokinase-type plasminogen activator to its receptor: residues involved in species specificity and binding. Arterioscler Thromb Vasc Biol 1998;18:693–701. [PubMed: 9598826]
38. Hallak LK, Merchan JR, Storgard CM, Loftus JC, Russell SJ. Targeted measles virus vector displaying echistatin infects endothelial cells via alpha(v)beta3 and leads to tumor regression. Cancer Res 2005;65:5292–5300. [PubMed: 15958576]
39. Andreasen PA, Kjoller L, Christensen L, Duffy MJ. The urokinase-type plasminogen activator system in cancer metastasis: a review. Int J Cancer 1997;72:1–22. [PubMed: 9212216]
40. Mandriota SJ, Seghezzi G, Vassalli JD, et al. Vascular endothelial growth factor increases urokinase receptor expression in vascular endothelial cells. J Biol Chem 1995;270:9709–9716. [PubMed: 7730348]
41. Prager GW, Breuss JM, Steurer S, et al. Vascular endothelial growth factor receptor-2-induced initial endothelial cell migration depends on the presence of the urokinase receptor. Circ Res 2004;94:1562–1570. [PubMed: 15131009]
42. Romer J, Nielsen BS, Ploug M. The urokinase receptor as a potential target in cancer therapy. Curr Pharm Des 2004;10:2359–2376. [PubMed: 15279614]
43. Li Y, Cozzi PJ. Targeting uPA/uPAR in prostate cancer. Cancer Treat Rev 2007;33:521–527. [PubMed: 17658220]
44. Paraskevakou G, Allen C, Nakamura T, et al. Epidermal growth factor receptor (EGFR)-retargeted measles virus strains effectively target EGFR-or EGFRvIII expressing gliomas. Mol Ther 2007;15:677–686. [PubMed: 17299404]
45. Ungerechts G, Springfeld C, Frenzke ME, et al. An Immunocompetent Murine Model for Oncolysis with an Armed and Targeted Measles Virus. Mol Ther 2007;15:1991–1997. [PubMed: 17712331]
46. Jain RK. Vascular and interstitial barriers to delivery of therapeutic agents in tumors. Cancer Metastasis Rev 1990;9:253–266. [PubMed: 2292138]
47. Liu Y, Deisseroth A. Tumor vascular targeting therapy with viral vectors. Blood 2006;107:3027–3033. [PubMed: 16373660]
48. Seghezzi G, Marelli R, Mandriota SJ, Nolli ML, Mazzieri R, Mignatti P. Tumor cell-conditioned medium stimulates expression of the urokinase receptor in vascular endothelial cells. J Cell Physiol 1996;169:300–308. [PubMed: 8908197]
49. Bianchi E, Cohen RL, Thor AT, et al. The urokinase receptor is expressed in invasive breast cancer but not in normal breast tissue. Cancer Res 1994;54:861–866. [PubMed: 8313371]

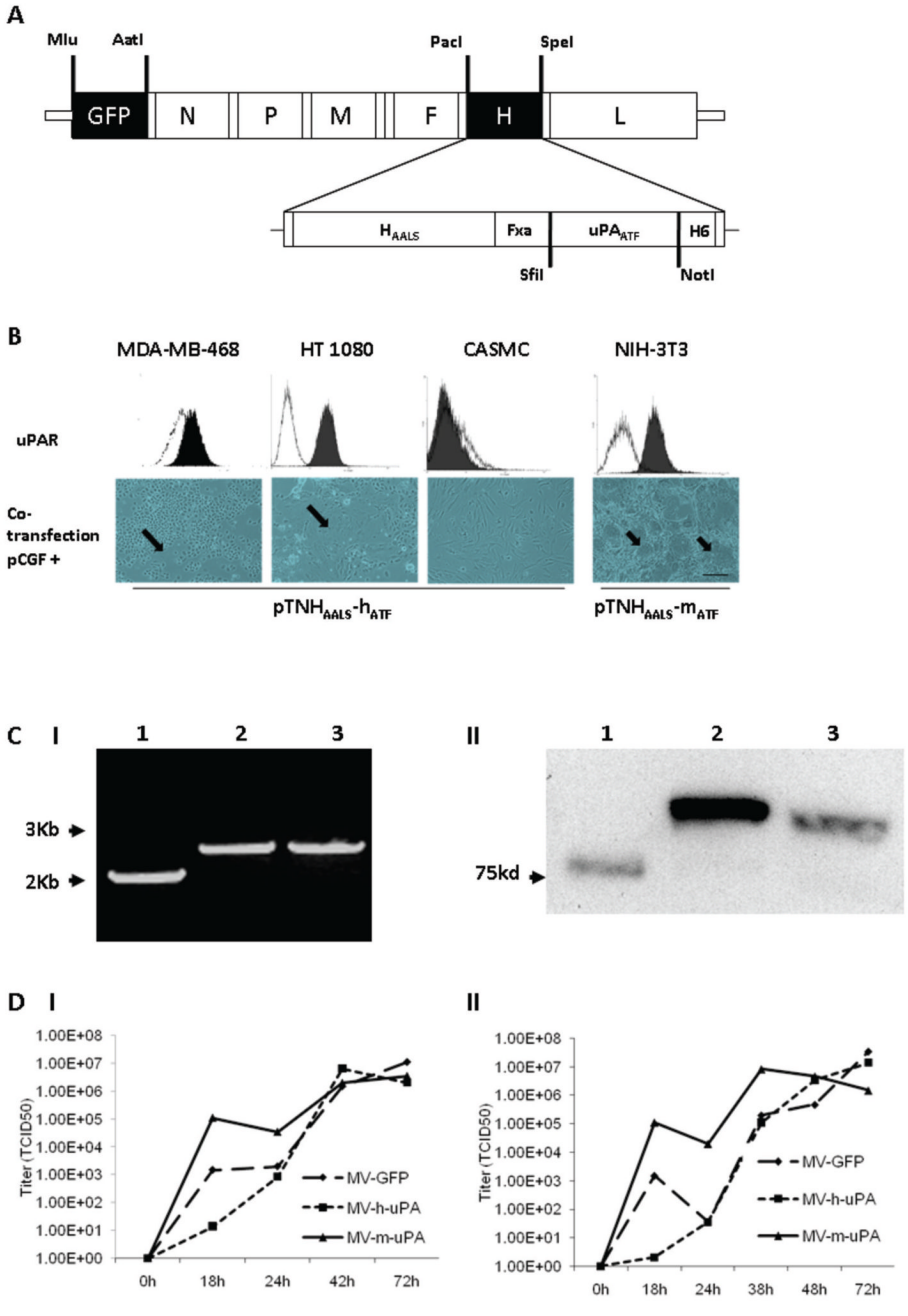

Figure 1. Rescue and in vitro characterization of recombinant oncolytic measles viruses fully retargeted against human and murine uPAR

(A) Schematic representation of the recombinant retargeted measles virus genome. The amino terminal fragment (ATF) of human or murine uPA, flanked by the *Sfi*I/*Not*I restriction sites was displayed as a C-terminal extension of H_{AALS}, a measles virus H glycoprotein with 4 residue mutations (AALS: Y481A, R533A, S548L, F549S) that ablate its ability to bind CD46 and SLAM (32). **(B)** Functional fusion formation assay of chimeric MV-H glycoproteins. After assessing expression of human (MDA-MB-468, HT-1080 and CASMC cells) and murine (NIH-3T3) uPAR by FACS (upper panel), cells were cotransfected with pCGF, a mammalian expression vector encoding MV-F (fusogenic) glycoprotein and either $pTNH_{AALS}$-h-ATF

(MDA-MB-468, HT1080 and CASMC) or pTNH$_{AALS}$-m-ATF (NIH-3T3). Cell fusion was observed in the human (MDA-MB-231, HT1080) and murine (NIH-3T3) tumorigenic cells (arrows), but not in non-cancer cells (CASMC) 48 hours after cotransfection. Scale bar = 500 μm. After confirming functional activity of H$_{AALS}$-ATF (human and murine), the chimeric glycoproteins were cloned individually into the *Pac*I/*Spe*I sites of the measles virus genome (Fig. 1A). The human and murine retargeted viruses were named MV-h-uPA and MV-m-uPA, respectively. The enhanced green fluorescent protein (eGFP) gene was inserted into the *Mlu*/*Aat*I site before the N gene. Fxa= factor Xa cleavage site (IEGR). H6= six-histidine peptide. N= nucleocapsid, P= phosphoprotein. M= matrix; F= fusion. H= hemagglutinin; L= polymerase gene. **(C)**. **I**, RT-PCR analysis of MV-H glycoproteins in uPAR retargeted MVs (Left panel). *Lane 1*, MV-GFP; *lane 2*, chimeric MV-m-uPA; *lane 3*, MV- h-uPA. **II**, Immunoblot analysis of viral H protein using anti-H antibody. Equal titers of each virus were loaded. *Lane 1*, unmodified control H protein with mobility at 75 kDa; *lane 2*, chimeric MV-m-uPA; *lane 3*, MV- h-uPA. **(D)**. In vitro viral propagation analysis of MV-h-uPA and MV-m-uPA by the one step growth curve in Vero-αHis cells. Titers (TCID50) of retargeted viruses were comparable to the unablated control virus (MV-GFP). **I**, Cell associated virus; **II**, cell released virus.

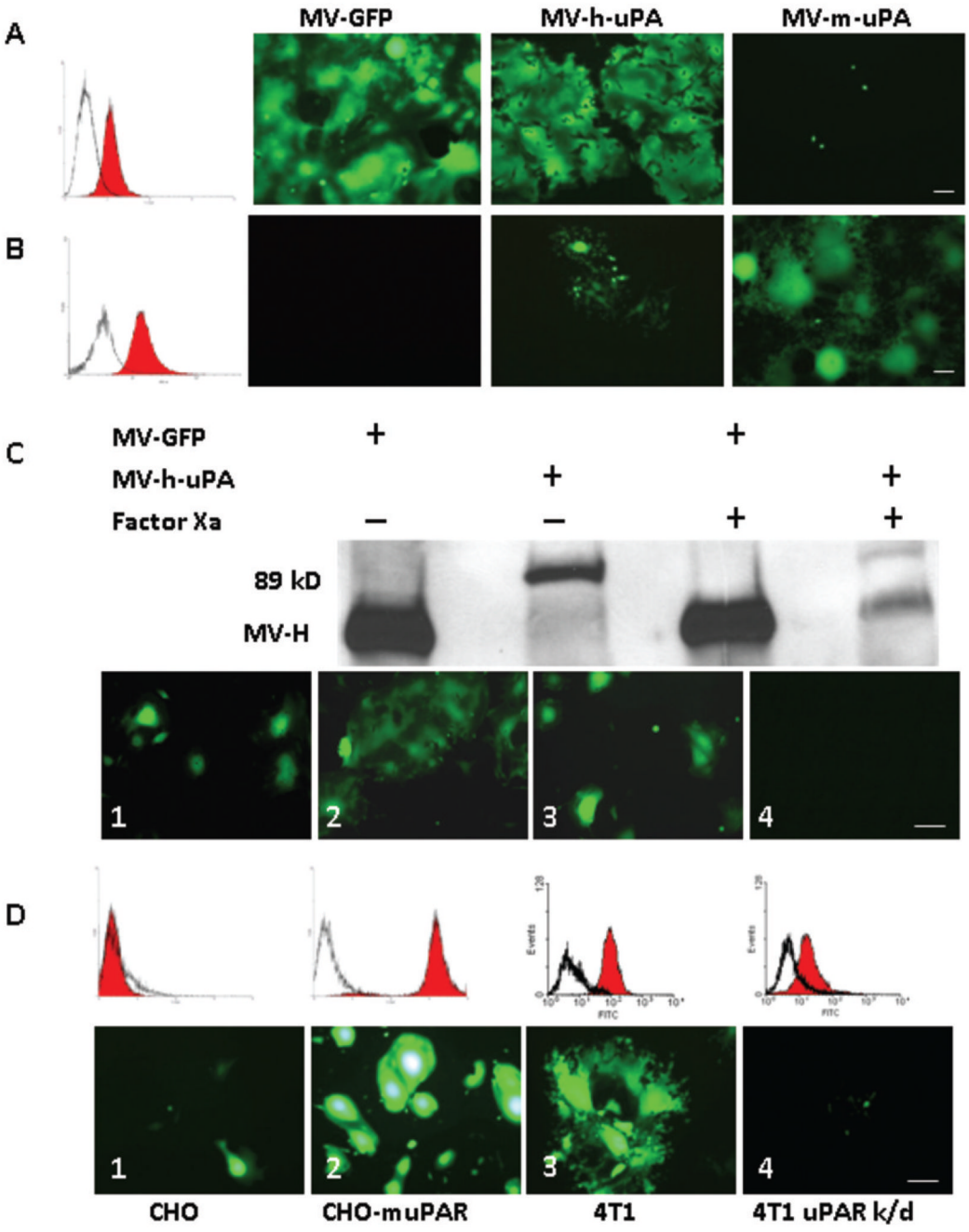

Figure 2. Receptor and species specificity of MV-uPA

uPAR expression in human MDA-MB-231 **(A)** and MC-38 **(B)** was assessed with human and murine anti-uPAR monoclonal antibodies (filled histograms) or isotype controls (open histograms). Cells were infected with each of recombinant measles viruses as indicated at an MOI of 0.5 and photographed 48 h after infection. MDA-MB-231 cells (A) underwent cell fusion after MV-GFP and MV-h-uPA infection, but not with MV-m-uPA. Conversely, MC-38 cells **(B)** were resistant to unmodified MV-GFP and MV-h-uPA (isolated green cells but not significant syncytia were observed-due to some degree of cross reactivity between human and mouse uPAR) and sensitive to MV-m-uPA. **C**. The chimeric MV-H-ATF glycoproteins contain a (coagulation) factor X(a) cleavage linker (*IEGR*) (32), before the *Not*I restriction site (Fig.

1. A). An aliquot of MV-GFP or MV-h-uPA viral particles was pretreated with 20 μg/mL of activated factor X [FX(a)] (New England Biolabs, Beverly, MA) or PBS (mock treatment) for 30 minutes at room temperature, in sterile conditions, before infection of MDA-MB-231 cells. Western blot analysis shows successful factor X(a) induced cleavage of the linker and detachment of the uPA-ATF from the H glycoprotein (western blot, far right lane). Untreated MV-GFP and MV-h-uPA (MOI= 0.5) induced cell fusion in MDA-MB-231(Lower panel, C. 1, MV-GFP; C.2, MV-h-uPA). Factor X(a) treatment of MV-GFP did not affect cell fusion (C. 3). Factor X(a) treatment of MV-h-uPA prevented fusion and syncytia formation in MDA-MB-231 cells (C.4). **D**. Chinese hamster ovary (CHO) cells stably overexpressing murine uPAR (D.2) underwent fusion and syncytia formation after infection with MV-m-uPA, compared to wild type CHO cells (D.1). D.3. 4T1 cells express murine uPAR and undergo fusion after infection with MV-m-uPA (MOI=1). uPAR expression in this cell line was knocked down by a retroviral vector encoding microRNA-based shRNA against mouse uPAR. uPAR expression was significantly decreased as determined by real time PCR (data not shown) and by flow cytometry (86% decrease, as assessed by FACS analysis of uPAR). uPAR knockdown (D.4) of 4T1 cells reduces the ability of MV-m-uPA to induce cell fusion. Scale bar = 100 μm.

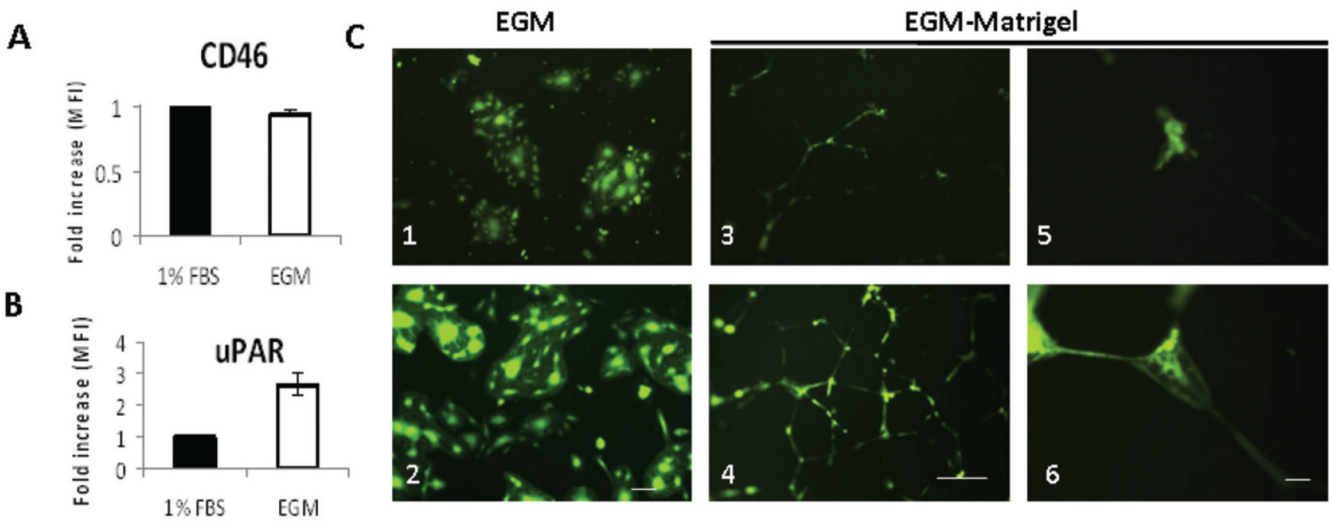

Figure 3. uPAR dependent in vitro endothelial cell infection

HUVECs were grown in full endothelial growth medium (EGM-2) (stimulated) or in EBM-2 medium with 1% FBS (unstimulated). Stimulation of HUVEC monolayers with 2% serum and growth factors (endothelial growth medium, EGM-2) was associated with upregulation of uPAR (**B**), but not CD 46 (**A**), compared to unstimulated HUVECs (endothelial basal medium and 1% FBS). Changes in HUVEC expression of CD46 and uPAR were determined by FACS analysis, and displayed as fold increase of mean fluorescence index (MFI) before and after stimulation. HUVEC monolayers were infected with viruses at an MOI=0.5. **C**. In stimulated HUVECs, MV-h-uPA induced cell fusion more efficiently than MV-GFP (C. 2, vs. C. 1). Scale bar = 100 μm. HUVECs (grown in EGM-2) were plated on matrigel and tubes were allowed to form (16 hours). Once tubes were formed, they were infected with either MV-GFP (C. 3, C.5) or MV-h-uPA (C. 4, C. 6) at a MOI = 1. Pictures of the areas of abundant tubes mostly in the center of wells were taken at 72 hours after infection. MV-h-uPA was associated with more efficient capillary infection compared with the unmodified virus control (C. 4 and 6 vs. C. 3 and 5). Experiments were done in triplicate. Scale bar = 500 μm (C. 3, 4) and 50 μm (C. 5, 6).

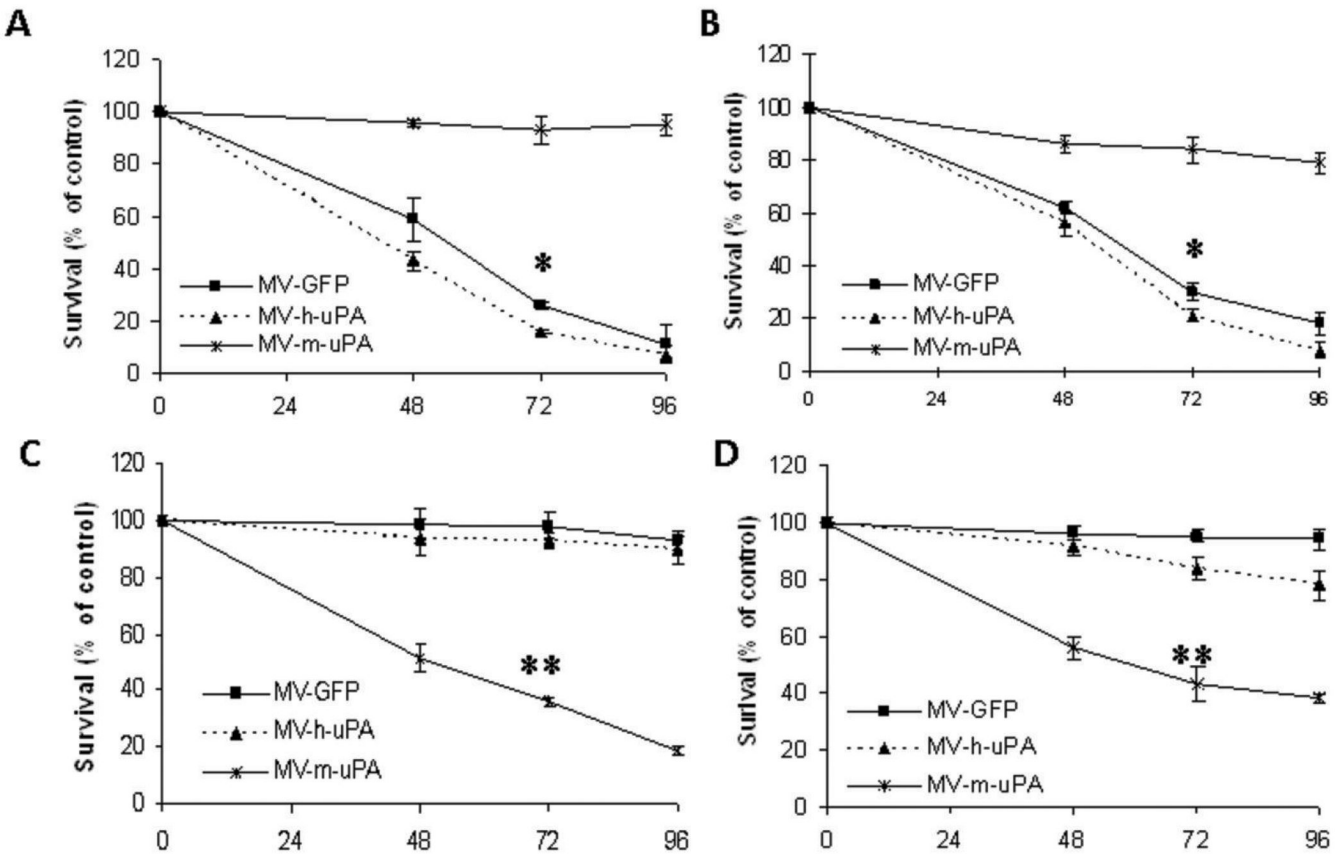

Figure 4. In vitro cytopathic effects of MV-uPA

Human and murine tumorigenic cells were infected with different viruses at an MOI=1 and viability was determined at different time points (48h, 72h, and 96h) by trypan blue exclusion and presented as percentage of uninfected cells. Human cancer cell lines MDA-MB-231 (**A**) and 786-O (**B**) underwent significant cytotoxicity when treated with MV-h-uPA at 48, 72 and 96 hours. *$p < 0.001$ (MV-GFP, MV-h-uPA vs. MV-m-uPA at 72h. **C, D**. MV-m-uPA induced significant cytotoxicity in the murine tumorigenic cell lines 4T1 (C) and 3T3-Ras (D). Murine cell lines were resistant to MV-GFP and MV-h-uPA, as they do not express human CD46 or human uPAR. *= $p < 0.001$ MV-m-uPA vs. MV-GFP and MV-h-uPA at 72 hours.

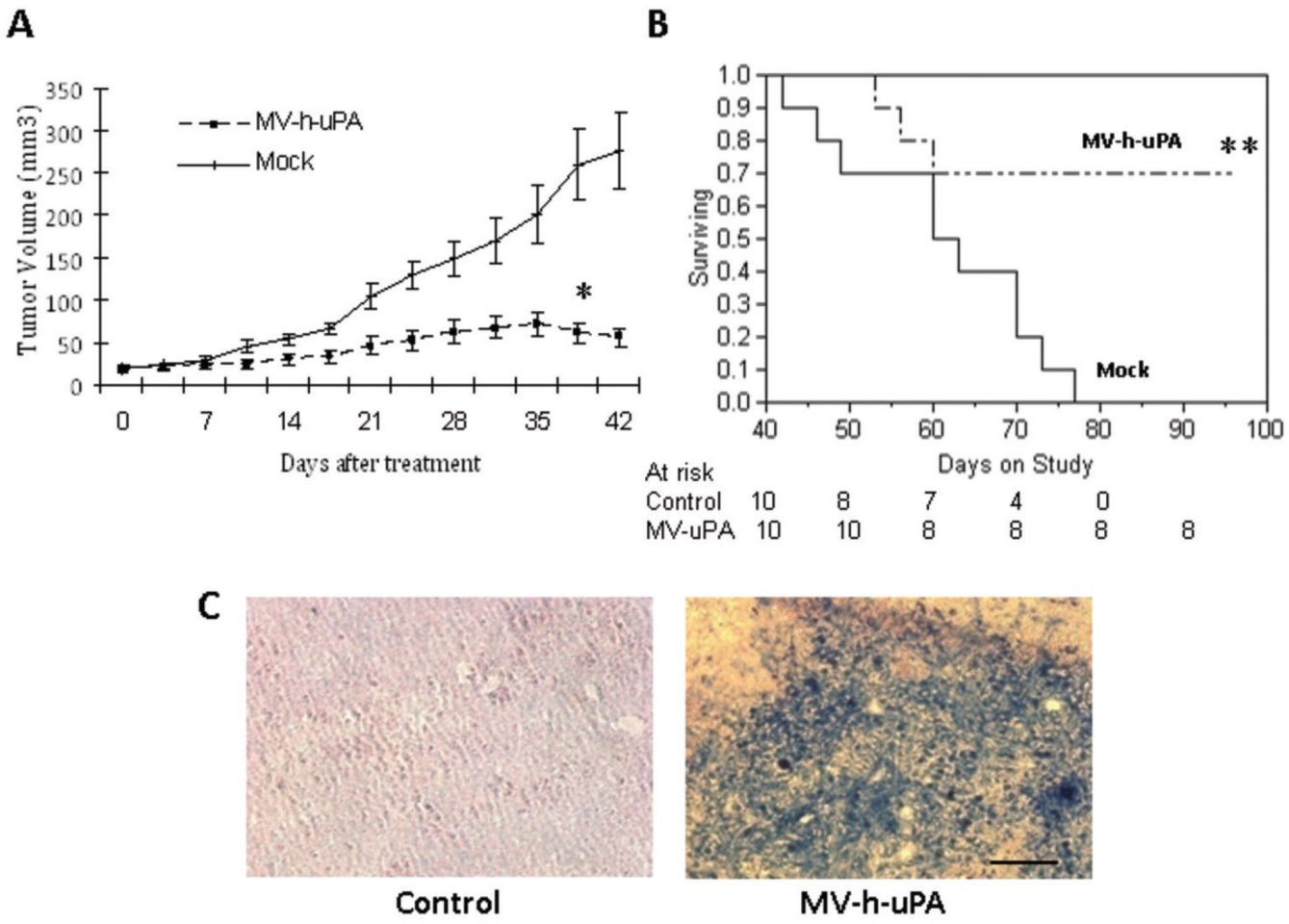

Figure 5. In vivo antitumor effects and tumor targeting

(A). MDA-MB-231 xenografts were established orthotopically by implantation of MDA-MB-231 into the mammary fat pad of female NOD/SCID mice. When the tumors reached a mean diameter of 0.4–0.5 cm, the animals (ten per group) were treated with 7 doses of MV at a dose of 1×10^6 $TCID_{50}$ intravenously per dose. Mice in the mock therapy group were injected with equal volumes of Opti-MEM. **A**. Systemic MV-h-uPA treatment was associated with a significant retardation in tumor growth compared to controls. *p= 0.0009 (Wilcoxon ranks sum test). **(B)**. Kaplan-Mier analysis of survival of tumor bearing mice treated with vehicle control or MV-h-uPA. Mice were monitored until they reached sacrifice criteria (see materials and methods). There was a significant prolongation of survival in the MV-h-uPA treatment group compared with control. **p= 0.0039 (Log Rank Test) **(C)**. In vivo experiments for detection of measles virus. In separate experiments, tumor bearing mice injected twice intravenously (n = 3 per group) with 2×10^6 $TCID_{50}$ viruses. Tumors were harvested 3 days later and frozen tumor sections were used for immunostaining for measles N protein. Viral protein was detected in the tumors after intravenous administration of the virus. Scale bar = 100 μm.

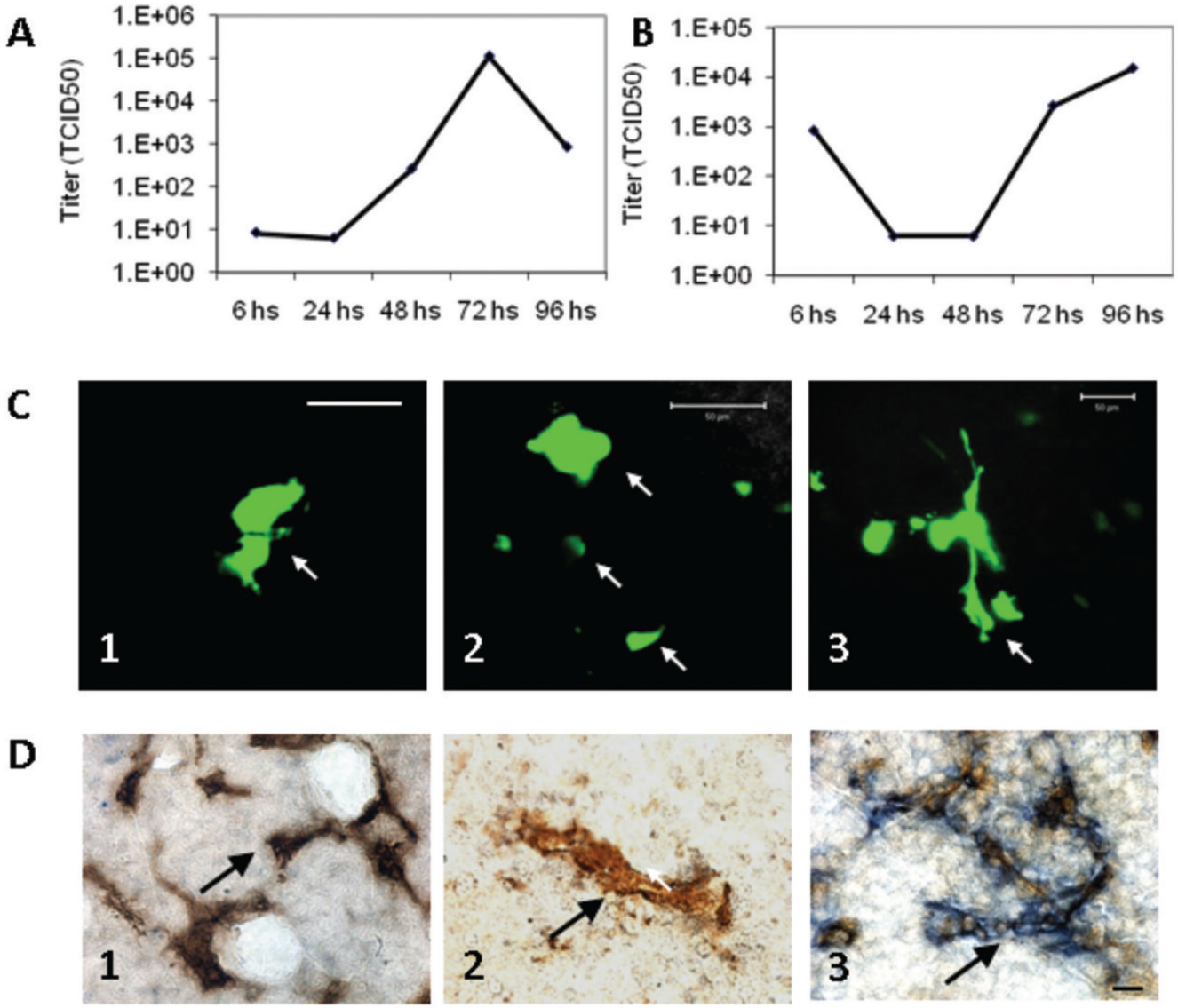

Figure 6. MV-m-uPA replicates in murine cells and transduces murine tumors and tumor vasculature in vivo

NIH-3T3 cells (which naturally express murine uPAR) were infected with MV-m-uPA (MOI=3) and titers of cell associated (**A**) and released (**B**) virus were determined at different time points by the one-step growth curve. Both cell associated and released virus titers increased over time, demonstrating in vitro viral replication in murine cells. **C**. 4T1 cells were implanted into the mammary fat pad of female immunocompetent (n = 3) and immunodeficient (SCID; n = 3) Balb/C mice. When tumors reached 5 mm, two intratumor injections of MV-m-uPA were administered to mice, and tumors were resected 48–72 hours later. In vivo viral transduction (determined by intratumor GFP expression) was evaluated by laser confocal microscopy of freshly resected tumor sections. GFP positive areas (arrows) consistent with intratumoral syncytia were observed in treated mice (C. 1, 2= SCID and C. 3= immunocompetent mice). Green tubular structures were also observed, suggesting infection of tumor capillary structures (C. 3). Scale bar= 50 μm. **D**. In vivo tumor vascular targeting. Mice bearing MDA-MB-231 tumors were injected systemically with MV-m-uPA (which targets murine uPAR) or MV-GFP, and double staining of tumor capillaries (MV-N protein

and CD31) was performed on resected tumors, after two treatments with intravenous MV-m-uPA. After systemic administration of MV-m-uPA in tumor bearing mice, strong blue staining for MV-N protein was observed around tumor capillaries (blue and brown staining, D. 3, arrows). No significant MV-N staining was observed in tumor capillaries (arrows) in mice treated systemically with MV-GFP (D. 2) or with vehicle control (D. 1). Additional pictures are available in supplementary fig. S.3. Scale bar = 10 μm.